PHILOSOPHICAL TRANSACTIONS OF THE ROYAL SOCIETY A MATHEMATICAL, PHYSICAL & ENGINEERING SCIENCES

Reversible adaptive regularization: perturbed Kepler motion and classical atomic trajectories

Benedict Leimkuhler

Phil. Trans. R. Soc. Lond. A 1999 **357**, 1101-1133
doi: 10.1098/rsta.1999.0366

THE ROYAL SOCIETY

Reversible adaptive regularization: perturbed Kepler motion and classical atomic trajectories

By Benedict Leimkuhler

Department of Mathematics, 405 Snow Hall, University of Kansas, Lawrence, KS 66045, USA (leimkuhl@math.ukans.edu)

Reversible and adaptive integration methods based on Kustaanheimo–Stiefel regularization and modified Sundman transformations are applied to simulate general perturbed Kepler motion and to compute classical trajectories of atomic systems (e.g. Rydberg atoms). The new family of reversible adaptive regularization methods also conserves angular momentum and exhibits superior energy conservation and numerical stability in long-time integrations. The schemes are appropriate for scattering, for astronomical calculations of escape time and long-term stability, and for classical and semiclassical studies of atomic dynamics. The components of an algorithm for trajectory calculations are described. Numerical experiments illustrate the effectiveness of the reversible approach.

Keywords: time-reversible variable step sizes; Hamiltonian systems; *N*-body problems

1. Introduction

This paper describes the design of efficient time-reversible regularized adaptive methods for long-term integration of coulombic few-body problems. The stable computation of trajectories is important for astronomical applications (Heggie 1988; Lecar 1968; Aarseth 1985) and in the classical and semiclassical studies of atomic systems, particularly atoms in highly excited ('Rydberg atom') states (Gu & Yuan 1993; Richter & Wintgen 1990; Ezra *et al.* 1991; Noid *et al.* 1986; Lee *et al.* 1997; Main & Wunner 1997; Gutzwiller 1990; Richter *et al.* 1993). Calculations of relevant stochastic quantities (average escape time, orbital dimension, etc.) may require long-time integrations. Using traditional methods, very small time-steps or non-physical corrective measures—such as rescaling of velocities—are sometimes needed to maintain roughly constant energy throughout a long simulation.

While the preservation of symplectic structure is known to lead to improved conservation of energy in long-term simulations (Sanz-Serna & Calvo 1994; Hairer 1994; Benettin & Giorgilli 1994; Hairer & Lubich 1999), we show that, at least in two-body scattering, discrete conservation of the symmetry and time-reversal symmetry implies an orbital axial symmetry which again confers superior energy conservation. Although this result is restricted to the two-body case, our numerical experiments suggest that the property is potent enough to facilitate stable long-term integration of perturbed Kepler motion and atomic few-body problems when a splitting technique is used to isolate the strong two-body contributions of the motion. Our method also conserves angular momentum.

Although some of the observations of this paper would be applicable to other types of systems, we will focus on N-body problems with a Hamiltonian

$$H = \sum_{i=1}^{N} \frac{|p_i|^2}{2m_i} - V(q).$$

Here $V(q)$ is a potential energy function that is assumed to decompose into coulombic two-body interactions:

$$V(q) = \sum_{i=1}^{N-1} \sum_{j=i+1}^{N} \frac{\alpha_{ij}}{r_{ij}}.$$

For gravitation, all of the coefficients α_{ij} are negative, whereas for atomic problems, both signs occur. To simplify the presentation, we will typically assume unit masses and that the constants α_{ij} are ± 1.

For atomic problems, the nuclei may often be assumed fixed in space to a first approximation, resulting in a reduced Hamiltonian for the electron motion.

The two types of coulombic problems are similar in that there are always some negative force coefficients α_{ij}. This makes possible arbitrarily close approaches of two bodies ('collisions') that are ruled out in other N-body systems such as molecular dynamics (due to Pauli repulsion). Gravitation and classical atomic dynamics differ in that three-body collisions, although rare in gravitation (Siegel & Moser 1971), are rarer still in atomic systems. For example, the only way to have a three-body collision in helium is along a zero-angular momentum orbit when the two electrons approach the nucleus from either side. This article focuses on the treatment of perturbed Kepler motion and atomic problems, i.e. problems without close three-body approaches.

Time transformations alone can be used as smoothing transformations for two-body collisions (Huang & Leimkuhler 1997; Hut *et al.* 1995); however, much better results are obtained when they are combined with various types of coordinate transformations (Kustaanheimo–Stiefel (KS) transformation, semiparabolic coordinates, etc.). These have the effect of reducing the pure Kepler problem to a linear system. When the KS transformation is used to generate a time-stepping method in the context of perturbations, the key problem turns out to be the efficient resolution of the time variable. We take up these issues in § 4. One component of our overall method is a regularizing energy-conserving symplectic Kepler solver that is more efficient than a standard quadrature.

Even with regularization, time transformations *per se* are still very important for two reasons: (1) we find that despite the use of a regularizing transformation, the *sensitivity* of the Keplerian motion to distant perturbing forces increases substantially during a collision; and (2) they are needed for treating the still quite strong forces, such as electron–electron interactions, which are not regularized by the KS transformation. Our method therefore also includes the use of an outer modified Sundman transformation incorporating these effects. A third use for the Sundman transformation is to automatically reduce the step size during very large motions such as those that occur during ionization in an external field.

The glue that binds all these techniques together is the fully explicit adaptive Verlet method (Holder *et al.* 1998), which allows us to incorporate the Sundman transformation in such a way that the overall time-stepping strategy preserves the time-reversal symmetry of the true flow. Although symplecticness is then sacrificed,

our experiments (see also Hut *et al.* 1995; Funato *et al.* 1996) show that this conservation is adequate to recover long-term behaviour reminiscent of symplectic methods. While experiments in Barth *et al.* (1999) with Lennard–Jones spheres suggested the possibility of instability in explicit variants of the adaptive Verlet method, we do not observe any such problems in the current application provided the control is properly chosen, probably because the adaptive Verlet scheme is only being used to control time-step with respect to (relatively) soft forces, after the collisions have been ameliorated by regularization.

A recent paper appearing in the astrophysics literature (Funato *et al.* 1996) describes a method for combining the KS transformation with time-reversible step-size variation for treating perturbed Kepler motion. This study did not consider multiple-body problems and it uses the implicit step-size variation technique of Hut *et al.* (1995) instead of an explicit scheme such as that described here; for this reason, we believe that our method will prove to be substantially more efficient in highly collisional problems. For three-body gravitation, an alternative symplectic approach to regularization has recently been suggested by Mikkola (1997).

The layout of the paper is as follows. In § 2, we discuss the energy error when a simple scattering problem is solved with various numerical methods, and point out that even the short-term dynamics of a collisional problem benefit from a symplectic scheme. In § 3, we demonstrate with a numerical experiment that time-reversible schemes applied to the time-transformed equations of motion also give excellent energy conservation, and we introduce the adaptive Verlet method. Section 4 discusses regularizing transformations and the fast Kepler solver. Section 5 discusses and compares several methods for treating perturbed Kepler problems. Section 6 describes the treatment of atomic systems based on splitting, the fast Kepler solver and the adaptive Verlet method. Section 7 revisits a scattering study that recently appeared in the physical literature; by using the new reversible adaptive regularization method, finer structure may be obtained in the regime of chaotic scattering.

All of the numerical experiments of §§ 5–7 were performed using the code SCAT, a C-language program available from the author for simulating perturbed Kepler motion and classical atomic trajectories. A companion article (Leimkuhler 1998) discusses the extension of the reversible adaptive regularization method for applied electrical and magnetic fields.

2. Background: symplectic methods in numerical scattering

In this section, we discuss the behaviour of various types of numerical integration methods when applied to a simple scattering problem, the Kepler problem with a Hamiltonian in polar coordinates given by

$$H = \tfrac{1}{2}p^2 - \frac{1}{q} + \frac{l^2}{2q^2}, \tag{2.1}$$

where $l = p_\theta$ is the angular momentum. The observations of this section generally apply to other collisional problems, such as the Kepler problem solved in Cartesian coordinates, or problems with purely repulsive potentials such as the Lennard–Jones molecular potential.

We integrate a fairly low-energy open orbit ($l = 0.5$, $H = 0.3975$) with six numerical methods (see Hairer *et al.* (1991) for details of the various methods). None of

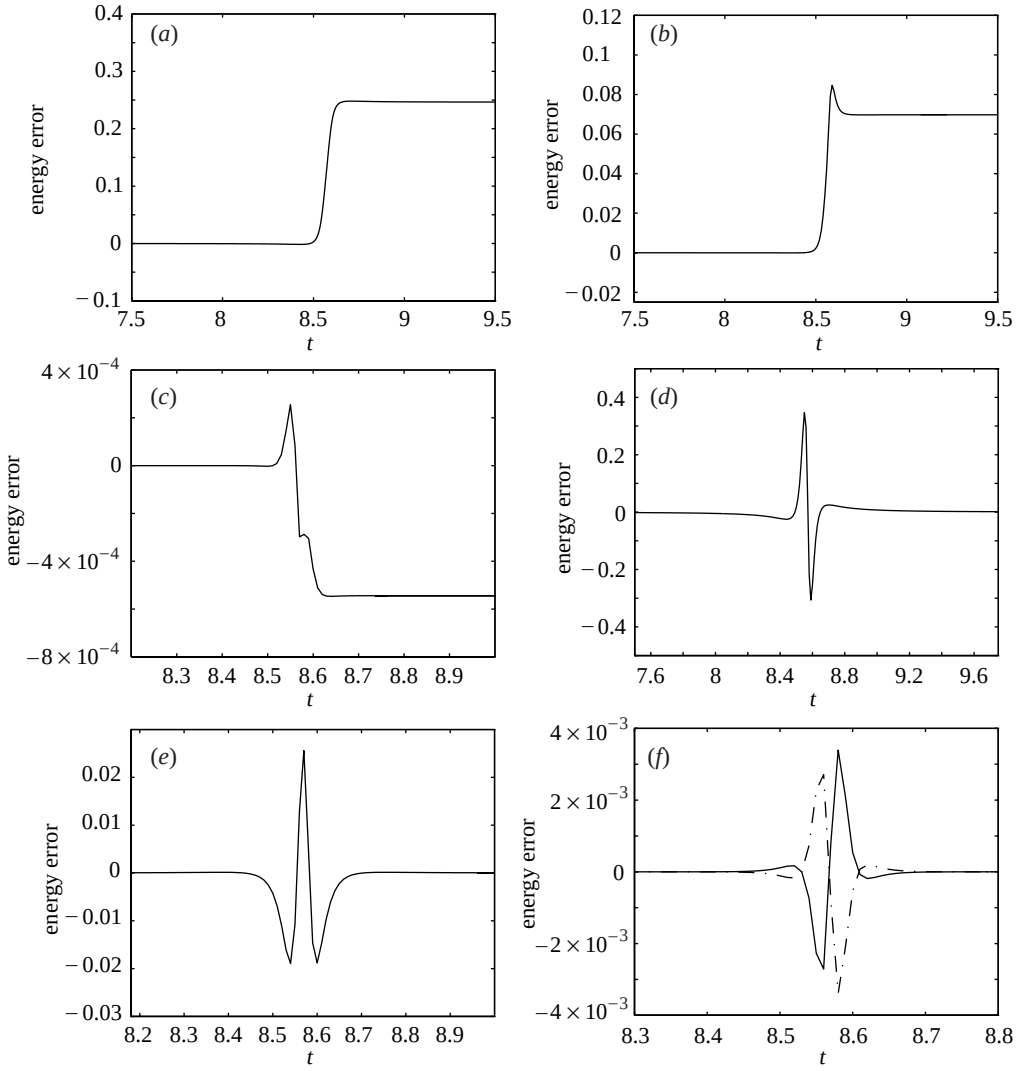

Figure 1. Energy profiles during two-body scattering: (*a*) Euler's method; (*b*) Heun's method; (*c*) fourth-order Runge–Kutta; (*d*) symplectic Euler; (*e*) leapfrog/Verlet; (*f*) third-order Ruth method (– · – · –) and the 'adjoint' method (——). Step size for Euler's method $\Delta t = 0.001$; all others used $\Delta t = 0.01$.

these schemes is energy-conserving, so we expect the energy to fluctuate with time, especially in the vicinity of the closest approach to the fixed body.

The graphs of numerical energy are shown in figure 1. For all of the six methods, energy variation is mild until perihelion, where one observes a sudden rapid variation. Qualitatively, the picture does not depend much on the step size or other parameters. In the first three methods, the energy does not return to the precollision level, whereas for each of the last three methods, the energy exhibits a remarkable stability through the collision, generally returning to very near the precollision energy level. Methods which have this property prove to be very effective for long-time-interval

computations. The difference between the methods is that the first three are all non-symplectic methods, while the last three are all symplectic, i.e. they preserve the wedge product of differentials at each time-step:

$$\mathrm{d}q_{n+1} \wedge \mathrm{d}p_{n+1} = \mathrm{d}q_n \wedge \mathrm{d}p_n.$$

The drift can be explained with the aid of the *modified equations* (Warming & Hyett 1974), a system of differential equations whose exact solution agrees with the discretization to some arbitrary prescribed order.

Given an initial-value problem of the form

$$\frac{\mathrm{d}}{\mathrm{d}t}z = f(z), \qquad z(0) = z_0,$$

where f is a C^∞ vector field. We compute numerical trajectories using the pth-order numerical method

$$z_{n+1} = \Phi_{\Delta t}(z_n).$$

Here z_n is an approximation to $z(t_n)$, where $t_n = n\Delta t$.

The idea of the modified equations is to construct a flow which coincides with the numerical solution (to some arbitrary prescribed order). This can typically be done by matching terms in an asymptotic expansion in powers of Δt:

$$\tilde{f}_{\Delta t} = f + \Delta t f^{(1)} + \Delta t^2 f^{(2)} + \cdots .$$

We compute the terms in the expansion recursively by demanding that the solution $\bar{z}$ of

$$\frac{\mathrm{d}}{\mathrm{d}t}\bar{z} = \tilde{f}_{\Delta t}(\bar{z}), \qquad \bar{z}(0) = z_n$$

agrees with the numerical solution after one step to a given order in Δt.

The modified equations allow us to use continuous dynamical-systems concepts to analyse near-to-the-identity discrete maps. An important property of the modified equations is summarized in the following 'metatheorem': *the modified equations inherit integrals, symmetries, reversing symmetries and symplectic structure from the discretization*. Special cases of this result are proved in Sanz-Serna & Calvo (1994), Hairer (1994), Gonzales & Stuart (1996) and Reich (1999). The case of a reversing symmetry has been considered in Hairer & Stoffer (1997).

When the discretization scheme is symplectic, i.e.

$$\partial_z \Phi_{\Delta t}^{\mathrm{T}} J \partial_z \Phi_{\Delta t} = J, \qquad J = \begin{bmatrix} 0 & I \\ -I & 0 \end{bmatrix},$$

then the metatheorem implies the existence of a perturbed Hamiltonian expansion

$$\tilde{H}_{\Delta t}^{(k)} = H + \Delta t H^{(1)} + \cdots ,$$

whose exact solution agrees, to any prescribed order in Δt, with the numerical solution (Sanz-Serna & Calvo 1994). For example, in the case of the symplectic Euler method applied to (2.1), the first two terms of the perturbed Hamiltonian are

$$\tilde{H}_{\Delta t}^{(1)} = H - \tfrac{1}{2}\Delta t p\left(\frac{1}{q^2} - \frac{l^2}{q^3}\right).$$

More generally, we can compute the terms of the nearby Hamiltonian for a symplectic Runge–Kutta or partitioned Runge–Kutta method by appealing to the theory of

trees (Hairer 1994; Sanz-Serna & Calvo 1994), in which case the precise form of the individual terms can be described ('elementary Hamiltonians'). Still more generally, such a series can be shown to exist for *any* symplectic map which is a smooth perturbation of the identity (MacKay 1990; Benettin & Giorgilli 1994).

Fixing any finite number of terms, it is straightforward to show that each finite higher-order term (involving Δt^k, $k \geqslant 1$) of the modified equations includes a reciprocal power of q and hence vanishes as $q \to \infty$, but this is not quite the whole story since the series expansion does not usually converge. Benettin & Giorgilli (1994) recently carried out an asymptotic study of the perturbed Hamiltonian expansion to show that symplectic methods always have the property that the energy tends to within $O(\exp(-K/\Delta t))$ of the precollision energy following a scattering event. In the few-body problem, this strong conservation property (the existence of the perturbed Hamiltonian and its properties) apparently explains the superiority of symplectic methods compared to non-symplectic methods. However, it is important to recognize that the bound in terms of $O(\exp(-K/\Delta t))$ is only valid in an asymptotic sense, for small step sizes (for which the error is very small); at large step sizes, the energy variation is complex and unpredictable. For more details, see Benettin & Giorgilli (1994), Hairer & Lubich (1999) and Reich (1999).

Returning to figure 1*d*–*f*, we comment on the appearance of the graphs. For the symplectic Euler method it is easy to see that

$$\tilde{H}^{(1)}(q,-p) + \tilde{H}^{(1)}(q,p) = 2H(q,p) + O(\Delta t^2), \tag{2.2}$$

and hence

$$\tilde{H}^{(1)}(q,0) = H(q,0) + O(\Delta t^2),$$

and, using (2.2) together with $H(q,-p) = H(q,p)$, the Poisson bracket of H and $\tilde{H}^{(1)}$ satisfies†

$$\begin{aligned}\{H(q,p), \tilde{H}^{(1)}(q,p)\} &= -\{H(q,p), 2H(q,p) - \tilde{H}^{(1)}(q,-p)\} \\ &= -\{H(q,p), \tilde{H}^{(1)}(q,-p)\} + O(\Delta t^2).\end{aligned}$$

Let $\Psi(t)$ represent the energy at time t obtained by integrating the modified equations forward in time from a point $(q,p) = (q_*, 0)$ at $t = 0$. Then

$$\begin{aligned}\Psi(t) &= H(q_*,0) + \int_0^t \dot{H}\,\mathrm{d}s \\ &= H(q_*,0) + \int_0^t \{H(q,p), \tilde{H}^{(1)}(q,p)\}\,\mathrm{d}s + O(\Delta t^2).\end{aligned}$$

Integrating backward in time is equivalent (up to the change in the sign of p) to integrating forward in time using the Hamiltonian $\tilde{H}^{(1)}(q,-p)$; thus,

$$\begin{aligned}\Psi(-t) &= H(q_*,0) + \int_0^t \{H(q,p), \tilde{H}^{(1)}(q,-p)\}\,\mathrm{d}s + O(\Delta t^2), \\ &= H(q_*,0) - \int_0^t \{H(q,p), \tilde{H}^{(1)}(q,p)\}\,\mathrm{d}s + O(\Delta t^2).\end{aligned}$$

† The Poisson bracket $\{f,g\} := \nabla_q f \cdot \nabla_p g - \nabla_p f \cdot \nabla_q g_q$ of functions $f = f(q,p)$, $g = g(q,p)$ can be viewed as the time rate of change of a function f along a trajectory of the Hamiltonian system with Hamiltonian g.

Finally,

$$\tfrac{1}{2}(\Psi(t) + \Psi(-t)) = H(q_*, 0) + O(\Delta t^2),$$

which explains the antisymmetric appearance of the observed energy curve in figure 1*d*. Higher-order symplectic methods would have a more complicated energy profile even in the leading term. An example is the third-order Ruth method (Ruth 1983) whose energy is shown in figure 1*f* (the adjoint method is also shown).

A more popular symplectic method for N-body calculations is the leapfrog or Verlet integrator. This method also respects the time-reversal symmetry typically present in physical systems:

$$\Phi_{\Delta t} \circ R = R \circ \Phi_{-\Delta t},$$

where

$$R\left(\begin{bmatrix} q \\ p \end{bmatrix}\right) = \begin{bmatrix} q \\ -p \end{bmatrix}.$$

This fact is a consequence of the fact that the adjoint method, $\Phi^*_{\Delta t} := \Phi^{-1}_{-\Delta t}$, coincides with the method itself: $\Phi^*_{\Delta t} = \Phi_{\Delta t}$. The energy profile for the leapfrog method is shown in figure 1*e*. Note that where the graph of the energy of the symplectic Euler method is roughly antisymmetric about the point of collision, the graph of the leapfrog scheme is symmetric about this point. This follows from the fact that the perturbed Hamiltonian of the leapfrog method is, like the original Hamiltonian, invariant under the involution $p \to -p$, and hence an orbit crossing the symmetry plane (here the line $p = 0$) must be symmetric about that plane.

In the next section, we will see that the symmetry property of the energy graph in this application can be viewed as a consequence of just the preservation of symmetries of the differential equations.

3. Variable step sizes: a reversible method

It is natural to consider the use of a variable step-size method for solving a problem such as scattering for which the solution is subject to sudden catastrophic events. Yet the results of using standard (non-conserving) variable step-size methods are not much better than the results obtained for fixed step-size methods. An example of a simple but popular variable step-size method is the Runge–Kutta–Fehlberg 4(5) embedded pair scheme, as implemented in MATLAB4.0. This method computes the new step by (1) applying a fourth-order Runge–Kutta method; (2) computing a further fifth-order approximation using the computed values of the vector field; then (3) adjusting the step size so that the difference between the two methods is less than a prescribed tolerance. A typical energy profile is shown in figure 2*a*. The additional dynamics induced by the step-size selection strategy are rather complicated, so one cannot expect the energy profiles to scale in a simple way with the tolerance. Even if the method used is symplectic, a traditional step-size variation method will destroy the conservative property of the method (Calvo & Sanz-Serna 1993).

A better way to incorporate time-step variation in a conservative system is to use a time transformation which preserves structure.

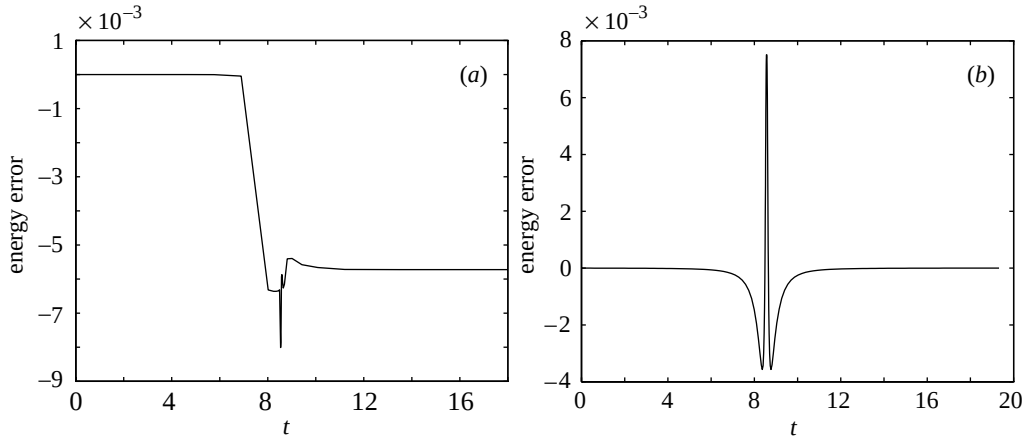

Figure 2. Energy profiles of variable step-size methods: (*a*) Runge–Kutta–Fehlberg 4(5), tolerance 0.001; (*b*) a reversible method based on implicit midpoint, fictive step $\Delta\tau = 0.2$.

(*a*) *Time transformations of Sundman and Poincaré*

A general Sundman transformation of time introduces a new 'artificial time' variable τ by

$$\frac{\mathrm{d}t}{\mathrm{d}\tau} = g(q,p),$$

where g is an arbitrary smooth, positive, scalar-valued function. The differential equations can then be written in terms of the independent variable τ as

$$\frac{\mathrm{d}}{\mathrm{d}\tau}q = g\nabla_p H,$$
$$\frac{\mathrm{d}}{\mathrm{d}\tau}p = -g\nabla_q H.$$

A solution of the scaled system is thus equivalent to that of the original system up to a reparametrization of time.

If the rescaled equations of motion are integrated with fixed step sizes $\Delta\tau$ in artificial time, it is as if the time-step was being adjusted according to the size of the scaling function g:

$$\Delta t \approx g\Delta\tau.$$

For Hamiltonian systems, it may be more appealing to use a *Poincaré transformation* of the form

$$\tilde{H} = g(q,p)(H - H_0),$$

where H_0 is the energy of a particular desired orbit. The differential equations corresponding to $\tilde{H}$ can be written as

$$\frac{\mathrm{d}}{\mathrm{d}\tau}q = g\nabla_p H + (H - H_0)\nabla_p g, \tag{3.1}$$
$$\frac{\mathrm{d}}{\mathrm{d}\tau}p = -g\nabla_q H - (H - H_0)\nabla_q g. \tag{3.2}$$

Note that along any particular orbit with energy $H = H_0$, the second term on the right-hand side of each of the differential equations will vanish and we are left with the Sundman transformed equations of motion. However, in the course of numerical integrations, there are typically some errors introduced in the energy, and the two approaches are then quite different.

The two types of time transformations provide different approaches to adaptive integration. If the discretization of the reparametrized equations preserves a geometric structure, then we can view the resulting method as a structure-preserving variable step-size method. For example, when the Poincaré transformation is used, then a symplectic step-size variation method can be obtained (Reich 1999; Hairer 1997); e.g. a symplectic second-order method is obtained by solving (3.1), (3.2) using the implicit generalized leapfrog discretization (Lobatto IIIA-B partitioned Runge–Kutta method) (Hairer 1997).

If a Sundman time transformation is positive and invariant under the involution $p \to -p$, then the rescaled equations of motion will possess the time-reversal symmetry, and use of an appropriate discretization scheme results in a time-reversible variable step-size strategy (Stoffer 1995; Hut *et al.* 1995; Huang & Leimkuhler 1997).

We will illustrate the use of the time-reversible method with the simple scattering problem. We take

$$\frac{\mathrm{d}t}{\mathrm{d}\tau} = g := \frac{q^2}{1+q^2}.$$

This time transformation is carefully chosen so that (1) at a close approach ($q \approx 0$) a unit step in τ corresponds to a very small step in t (proportional to $|q|^2$); while (2) when q is large the steps in t corresponding to fixed steps in τ remain bounded. Applied to the polar Kepler problem, the time transformation leads to the equations

$$\dot{q} = g(q)p,$$
$$\dot{p} = g(q)\left(-\frac{1}{q^2} + \frac{l^2}{q^3}\right).$$

These equations are no longer Hamiltonian, although the time-reversal symmetry is preserved. We solve the differential equations using the implicit midpoint method,

$$\bar{q} = q_n + \tfrac{1}{2}\Delta\tau g(\bar{q})\bar{p}, \qquad \bar{q} = \tfrac{1}{2}(q_n + q_{n+1}),$$
$$\bar{p} = p_n + \tfrac{1}{2}\Delta\tau g(\bar{q})\left(-\frac{1}{\bar{q}^2} + \frac{l^2}{\bar{q}^3}\right), \qquad \bar{p} = \tfrac{1}{2}(p_n + p_{n+1}),$$

and also update the time variable using this method:

$$t_{n+1} = t_n + \Delta\tau g(\bar{q}).$$

The approach described is not symplectic, yet its energy profile, shown in figure 2*b*, is similar to those of the symplectic schemes. This reflects a frequent observation in the literature: time-reversible integration schemes give excellent results in long-term integrations. For a general discussion of symmetries and reversing symmetries in discretization see McLachlan *et al.* (1998). For a recent example comparing symplectic, reversible and traditional integration methods for a large dimensional nonlinear physical problem (a Heisenberg ferromagnetic system), see Frank *et al.* (1997). While we do not have a complete understanding of why the reversible methods perform so well, we can give a fairly detailed explanation in the case of the Kepler problem where the symmetry of orbits is the key.

(*b*) *Orbital symmetry in scattering with reversible adaptive methods*

For the one-degree-of-freedom Kepler problem in polar coordinates, it is easy to see why the energy rebounds to the precollisional level when a reversible adaptive method is used. Observe that the modified equations (any finite truncation of the modified equations) must also possess the reversing symmetry (by the metatheorem stated in the last section). The orbit of the modified equations crosses the symmetry line $p = 0$, say at $q = q_*$. Integrating the equations forward in time from $(q_*, 0)$ or backwards in time from this point results in exactly the same trajectory up to the sign of p; hence the energy is also the same after integrating τ units either forward or backward in time, since H is an even function of p. This explains the symmetry observed in figure 2.

The argument does not immediately extend to the planar Kepler problem treated in the standard Cartesian coordinates, since orbits do not penetrate the symmetry plane $p_1 = p_2 = 0$. Nevertheless, an energy stability result can still be expected for the Kepler problem, provided both the time transformation and discretization preserve both the symmetry and time-reversal symmetry of the system. This result can be seen as an application of the analysis of Calvo & Hairer (1995) based on KAM theory for time-reversible maps, but for this special case, we prefer the following elementary explanation, which provides some additional insight.

After Sundman transformation, we have

$$\dot{q} = g(q,p)p, \tag{3.3}$$

$$\dot{p} = -g(q,p)q/|q|^3. \tag{3.4}$$

The Kepler problem ($g = 1$ in (3.3), (3.4)) possesses both a reversing symmetry $\mathcal{R} : t \to -t$, $p \to -p$, and symmetries of the form $\mathcal{S} : q \to Sq$, $p \to Sp$ for any orthogonal transformation S. (There is also an invariance under translation of time.) These symmetries are also preserved by the rescaled equations provided

$$g(q,p) > 0, \tag{3.5}$$

$$g(q,-p) = g(q,p), \tag{3.6}$$

$$g(Sq,Sp) = g(q,p), \quad SS^{\mathrm{T}} = I. \tag{3.7}$$

Not wishing to introduce an overly grandiose term for the property, a Sundman transformation preserving (3.5)–(3.7) will be termed *appropriate* for the Kepler problem. In particular, any $g = g(|q|) > 0$ is an appropriate Sundman transformation. Similarly, we will call a discretization scheme appropriate if it respects the symmetry and reversing symmetry of a given system.

In terms of a given orbit $O = \{(t, q(t), p(t))|t \in \mathbb{R}\}$ (figure 3*a*), the time-reversal symmetry means that $\mathcal{R}O = \{(t, q(-t), -p(-t))|t \in \mathbb{R}\}$ is also an orbit (figure 3*b*). The symmetry means that $\mathcal{S}O = \{(t, Sq(t), Sp(t))|t \in \mathbb{R}\}$, where $SS^{\mathrm{T}} = I$, is again an orbit. Note that the symmetry group includes both rotations and flips (figure 3*c*, *d*).

The orbits of the Kepler problem are *axially symmetric*, implying that there is a particular flip symmetry which, when followed by a time-reversal (and possibly a time translation), leaves the orbit invariant. The main result of this section is as follows.

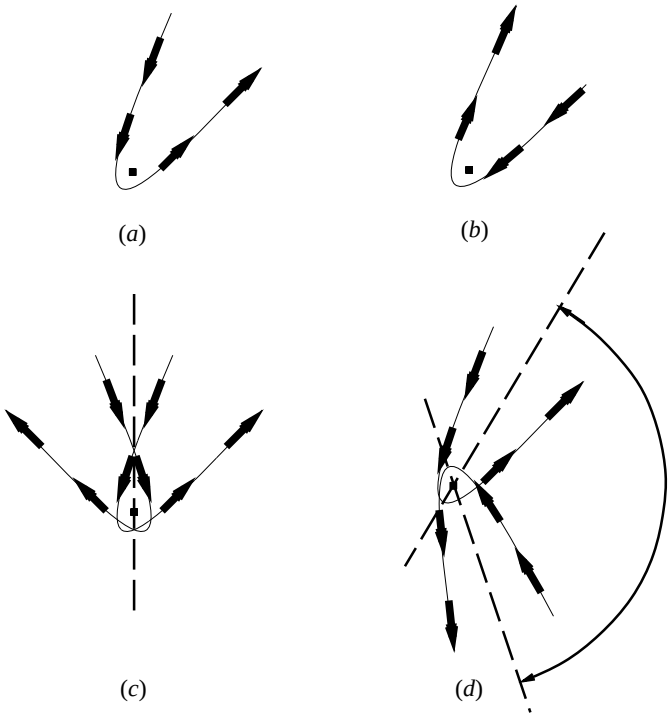

Figure 3. (*a*) A Kepler orbit; (*b*) its time-reversal; (*c*) a flip symmetry; (*d*) a rotational symmetry.

Theorem 3.1. *In the Kepler problem treated with an appropriate Sundman transformation and an appropriate discretization, every finite discrete orbit obtained with a sufficiently small time-step is axially symmetric.*

Proof. The proof relies on a variation of the metatheorem mentioned in § 1: namely that the modified equations for an appropriate discretization of the Kepler problem have the corresponding symmetry properties. The key problem is to identify an axis of symmetry for the discrete orbit. We sketch the proof for the case of a positive energy orbit ($H_0 > 0$).

Perihelion is distinguished by the orthogonality condition $q \cdot p = 0$; the latter quantity changes sign through a collision. Now, applying any appropriate Sundman transformation to the Kepler problem, one sees from (3.3), (3.4) that

$$\frac{\mathrm{d}}{\mathrm{d}t} q \cdot p = \tfrac{1}{2} g |p|^2 + g H_0 > 0,$$

and hence $q \cdot p$ is strictly monotone increasing along such an orbit. We can assume without loss of generality that the perihelion point ($q \cdot p = 0$) occurs at $t = 0$ (figure 4*a*).

Consider a convergent appropriate discretization method and an orbit

$$O = \{(t, \bar{q}(t), \bar{p}(t)) | t \in \mathbb{R}\}$$

of (a finite truncation of) the modified equations, which starts from some point $(-T, q(-T), p(-T))$ of the true orbit. Set $\bar{\mu}(t) := \bar{q}(t) \cdot \bar{p}(t)$.

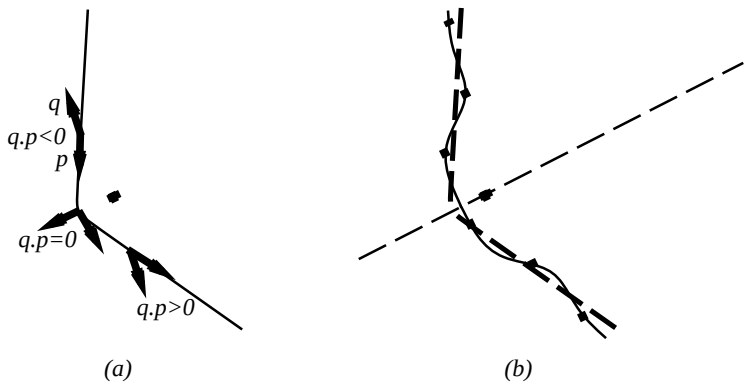

Figure 4. (*a*) $q \cdot p$ is monotone increasing; (*b*) an orbit (thick dashed line) with a numerical solution (boxes) and a corresponding orbit of the modified equations (thin solid line).

Since $q \cdot p$ is monotone in t, for a sufficiently small time-step, $\bar{\mu}$ must be monotone on $[-T, T]$ (by convergence) and will have a zero, say at $t = t_*$ and $(q_*, p_*) = (\bar{q}(t_*), \bar{p}(t_*))$. With perhaps a shift in time, we can assume without loss of generality that $t_* = 0$.

q_* now defines our axis of symmetry. Let $\mathcal{S}_*$ be the flip symmetry defined by the ray through q_*. That is, we define $\mathcal{S}_*$ as the linear plane symmetry described by the orthogonal transformation $S_* = 2q_* q_*^{\mathrm{T}}/|q_*|^2 - I$.

Applying the symmetry $\mathcal{S}_*$ to O, we get a new orbit. Applying the time-reversal symmetry $\mathcal{R}$ to O, we get yet another orbit. Clearly, $\mathcal{S}_* O$ includes the point $(0, q_*, -p_*)$, since $S_* q_* = q_*$, $S_* p_* = -p_*$. On the other hand, this point is also on the orbit $\mathcal{R}O$. By uniqueness of solutions to the initial-value problem, the two orbits must be equivalent. Thus, $\mathcal{S}_* O = \mathcal{R}O$, so $\mathcal{R}\mathcal{S}_* O = O$, and O is therefore axially symmetric (figure 4*b*). ■

The argument of theorem 3.1 implies that the energy variation, too, is symmetric with respect to the perihelion approach. The theorem could easily be extended to include arbitrary central-force two-body problems in $\mathbb{R}^3$, for which the solutions are planar and possess the same symmetry features.

The argument of theorem 3.1 breaks down, however, when three bodies interact at close range, and the energy can no longer be expected to return to very near its precollision value following such an event. Nonetheless, for the perturbed Kepler problem or, for that matter, the N-body problem, *orbits appear Keplerian in the vicinity of close approach* due to the local dominance of the coulombic force and the rarity of three-body collisions (Siegel & Moser 1971).

As we shall see in the following subsection, it is possible to formulate a powerful explicit scheme based on the reversible adaptive framework, and these methods can be quite powerful for N-body systems, especially when employed in combination with regularizing coordinate transformations.

(*c*) *The adaptive Verlet method*

The adaptive Verlet method of Huang & Leimkuhler (1997) provides a framework for discretizing the reparametrized equations in a reversible way. For a Hamiltonian

system of the form $H(p,q) = T(p) + V(q)$, a related fully explicit method consists of introducing a new variable ρ representing the reciprocal of the time-scaling factor and computed according to a symmetric recurrence relation. We then discretize by a three-stage scheme (Holder *et al.* 1998).

(I) Symplectic Euler half-step:

$$q_{n+(1/2)} = q_n + \frac{\Delta\tau}{2\rho_n}\nabla_p T(p_n),$$
$$p_{n+(1/2)} = p_n - \frac{\Delta\tau}{2\rho_n}\nabla_q V(q_{n+(1/2)}).$$

(II) Update of the scaling factor ρ via the formula

$$\rho_n + \rho_{n+1} = \frac{2}{g(q_{n+(1/2)}, p_{n+(1/2)})}. \tag{3.8}$$

(III) Symplectic Euler adjoint half-step:

$$q_{n+1} = q_{n+(1/2)} + \frac{\Delta\tau}{2\rho_{n+1}}\nabla_p T(p_{n+1})$$
$$p_{n+1} = p_{n+(1/2)} - \frac{\Delta\tau}{2\rho_{n+1}}\nabla_q V(q_{n+(1/2)}).$$

This method is a time-reversible generalization of Verlet (obtained when $g \equiv 1$). It also conserves the angular momentum of a system of particles. We sometimes use the method shifted by one half time-step, so that ρ is computed at the beginning, rather than in the middle, of each step. An asymptotic error analysis of the adaptive Verlet method may be found in Cirilli *et al.* (1999).

Note that the adaptive Verlet method is appropriate in the terminology of the last subsection.

The adaptive Verlet method is similar to the 'time-symmetrized' integrators discussed in Hut *et al.* (1995, 1999) and Funato *et al.* (1996), with a key difference: the latter methods are all based on an *implicit* formalism and require multiple force evaluations at a time-step if the nonlinear equations are to be solved to round-off and the method remains truly time-reversible.

Heggie (1974) suggested using time transformations alone to regularize N-body problems; his idea can be combined with the reversible schemes. Heggie used

$$g = 1/U,$$

where U is the potential energy. For the Kepler problem, this means $g = |q|$. In our experience this gives some improvement over the unmodified Kepler problem, but, for stable integration in the presence of perturbations, a much stronger transformation of the form

$$g = |q|^2$$

is needed to carry out integration near the close approaches. The use of such an approach based solely on time transformation is not efficient for even moderately difficult trajectories in our experience (see § 5).

In Rzazewski *et al.* (1994), the singularity of the coulombic potential is removed by incorporating a small parameter, i.e $1/r \to 1/(r+\epsilon)$. This changes the structure of phase space in a fundamental way and eliminates many complicated orbits. While

some justification is occasionally given for this type of 'smoothing' in atomic problems on physical grounds (for multielectron atoms, the perturbation can be viewed as induced by an excited electron in a close orbit around the nucleus (see Rzazewski *et al.* 1994)), we prefer an approach based on the use of a combination of coordinate and time transformations to regularize the closest two-body approaches.

4. Fast Kepler solver

A coordinate transformation $(q, p) \mapsto (Q, P)$ of the form

$$q = \phi(Q),$$
$$\phi'(Q)^{\mathrm{T}} p = P,$$

where ϕ is a diffeomorphism of $\mathbb{R}^N$, is called a 'cotangent lift transformation' (Marsden 1992). Such a map is always necessarily symplectic (canonical), meaning that $\sum_i \mathrm{d}q_i \wedge \mathrm{d}p_i \equiv \sum_i \mathrm{d}Q_i \wedge \mathrm{d}P_i$. Under such a transformation, the Hamiltonian becomes

$$\bar{H}(Q, P) = H(\phi(Q), \phi'(Q)^{-T} P).$$

For the purposes of numerical integration, we can use a lift transformation as follows: (1) map initial conditions (q_0, p_0) to (Q_0, P_0) under the transformation; (2) integrate the differential equations for the transformed Hamiltonian $\bar{H}$ for some desired time t; and (3) map the solution back under the inverse transformation. Usually, we will have to perform step (2) using some (ideally symplectic) numerical integration procedure.

The traditional way of regularizing two-body motion in N-body gravitational simulations is via the KS transformation. The idea is to introduce both coordinate and time transformations that reduce the two-body problem to a linear system which is then easily solved. In N-body simulations, the coordinate transformations have the effect of stabilizing the numerical dynamics. This method, which generalizes the planar Levi–Civita regularization, can be implemented in a canonical framework. In $\mathbb{R}^4$ we introduce the coordinate transformation

$$\begin{bmatrix} q \\ 0 \end{bmatrix} = \phi(Q) = \mathcal{L}(Q)Q, \tag{4.1}$$

where Q is a 4-vector and $\mathcal{L}(Q)$ is the KS matrix

$$\mathcal{L}(Q) = \begin{bmatrix} Q_1 & -Q_2 & -Q_3 & Q_4 \\ Q_2 & Q_1 & -Q_4 & -Q_3 \\ Q_3 & Q_4 & Q_1 & Q_2 \\ Q_4 & -Q_3 & Q_2 & -Q_1 \end{bmatrix} =: |Q|\mathcal{R}(Q),$$

with $\mathcal{R}$ an orthogonal matrix. The transformation has the property $|q| = |Q|^2$.

Note that

$$\phi'(Q) = 2\mathcal{L}(Q),$$

and hence the canonical momenta P to Q are related to p directly by

$$\phi'^{\mathrm{T}} \begin{bmatrix} p \\ 0 \end{bmatrix} = P \Rightarrow \begin{bmatrix} p \\ 0 \end{bmatrix} = \frac{1}{2|Q|}\mathcal{R}P. \tag{4.2}$$

The KS transformation introduces an S^1 symmetry through the following quadratic constraint on Q, P:

$$Q_4P_1 - Q_3P_2 + Q_2P_3 - Q_1P_4 = 0. \tag{4.3}$$

To put this another way, ϕ can be viewed as a map from the reduction of $\mathbb{R}^4$ modulo S^1 into $\mathbb{R}^3$. With this interpretation, the inverse map is well defined and easily computable (Kustaanheimo & Steifel 1965).

The Hamiltonian in the new variables is

$$H = \frac{1}{8}\frac{|P|^2}{|Q|^2} - \frac{1}{|Q|^2}.$$

After a Poincare-type time transformation, we get a linear Hamiltonian system:

$$\tilde{H} = |Q|^2(H - H_n) = \tfrac{1}{8}|P|^2 - 1 - H_n|Q|^2,$$

where H_n is the energy at the beginning of the time-step. It is important to ensure that the initial values for Q and P are chosen so as to satisfy the constraint (4.3), but this equation then becomes an integral invariant of the transformed system (so it is satisfied automatically by the true flow).

The Poincaré transformation introduces a nonlinear scaling of time, i.e. the equations of motion are

$$\frac{\mathrm{d}}{\mathrm{d}s}Q = \tfrac{1}{4}P, \tag{4.4}$$

$$\frac{\mathrm{d}}{\mathrm{d}s}P = 2H_nQ, \tag{4.5}$$

$$\frac{\mathrm{d}t}{\mathrm{d}s} = |Q|^2.$$

Resolving the motion thus requires propagation of Q, P as the flow of a simple linear system, coupled to the scalar differential equation

$$\frac{\mathrm{d}s}{\mathrm{d}t} = |Q(s)|^{-2}.$$

If the solution is needed at a fixed time T, the resolution of the corresponding fictive time $S(T)$ is non-trivial, requiring the computation and inversion of the antiderivative function for $|Q|^2$. To perform this calculation, we write

$$F(S) := T - \int_0^S |Q(s)|^2 \,\mathrm{d}s, \tag{4.6}$$

and apply scalar Newton iteration:

$$S^{(m+1)} = S^{(m)} - \frac{F(S^{(m)})}{F'(S^{(m)})}$$

$$= S^{(m)} + \frac{F(S^{(m)})}{|Q(S^{(m)})|^2}.$$

Since Q is determined by solving linear differential equations, the formulae can be greatly simplified; however, this calculation introduces some overhead in the form of transcendental functions which must be re-evaluated several times until convergence.

Since our method relies on very frequent computations of two-body problems, including resolution of the inverse time transformation, it becomes an expensive

component of the algorithm. We have found that an alternative approach using the implicit midpoint discretization to solve the KS-transformed equations together with the equation of time is reliable and substantially cheaper than using the exact quadrature. Specifically, we solve

$$Q_{n+1} = Q_n + \tfrac{1}{4}\Delta s P_{n+1/2}, \tag{4.7}$$

$$P_{n+1} = P_n + 2\Delta s H_n Q_{n+1/2}, \tag{4.8}$$

$$\Delta t = \Delta s |Q^{n+1/2}|^2, \tag{4.9}$$

$$Q_{n+1/2} = \tfrac{1}{2}(Q_n + Q_{n+1}),$$

$$P_{n+1/2} = \tfrac{1}{2}(P_n + P_{n+1}).$$

To solve this system, we write

$$Q_{n+1/2} = Q_n + \tfrac{1}{8}\Delta s(P_n + \Delta s H_n Q_{n+1/2}),$$

which gives an equation solvable for $Q_{n+1/2}$:

$$Q_{n+1/2} = (1 - \tfrac{1}{8}\Delta s^2 H_n)^{-1}(Q_n + \tfrac{1}{8}\Delta s P_n).$$

Hence, after computing the squared two-norm and substituting into the equation of the time-step (4.9), we arrive at

$$F(\Delta s) := (1 - \tfrac{1}{8}\Delta s^2 H_n)^2 \Delta t - \Delta s(|Q_n|^2 + \tfrac{1}{4}\Delta s Q_n \cdot P_n + \tfrac{1}{64}\Delta s^2 |P_n|^2) = 0. \tag{4.10}$$

The equations thus reduce to a fourth-degree polynomial equation for Δs, and no transcendental functions need to be evaluated. Although this quartic equation could be solved in radicals, it is much more economical to use a Newton iteration to resolve the time variable. As a stopping criterion for the Newton iteration, we used

$$\delta := |F/(\Delta s F')|, \qquad \delta/\text{RTOL} + |F|/\text{ATOL} < 1,$$

where, on a Pentium PC using double precision, $\text{RTOL} = 10^{-8}$, $\text{ATOL} = 10^{-11}$ worked well. Occasionally, we encountered difficulty with Newton convergence during very close approaches and suggest that a more robust modified Newton iteration (Bulirsch & Stoer 1980) should be used in software.

The Kepler solution (and the resolution of the time variable) represented a substantial component of overall CPU time in our experiments. In typical runs, the fast Kepler solver reduced the overall CPU time for the code by a factor of more than 1.5 compared to using the exact solution of (4.4), (4.5), although this difference is overshadowed by the extraordinary differences (discussed below in the numerical experiments) in performance of the regularizing scheme compared to methods using fixed steps or only a variable step size.

The implicit midpoint method is symplectic and preserves all quadratic first integrals, such as the energy in transformed variables and the special constraint (4.3)†. Except at extraordinarily close approaches to the fixed body (see § 7), we were unable to observe any substantive differences between algorithms based on exact quadrature and the fast Kepler solver in experiments, other than a substantial gap in performance. During very close approaches (within, say, 10^{-7}) the exact Kepler quadrature should probably be used for improved robustness.

† Observe that the simultaneous conservation of energy and symplectic structure is only an apparent contradiction of the famous theorem of Ge & Marsden (1988), since the conditions of that theorem specifically exclude integrable cases.

5. Perturbed Kepler motion

In this section, we will use the KS transformation to treat perturbed Keplerian motion, while taking advantage of the superior conservation properties of reversible adaptive integrators. The idea is to find a way to separate appropriately the computation of the Keplerian dynamics from the perturbation within a time-step. Our approach also takes advantage of the fast Kepler solver and the time transformations mentioned in the previous sections to handle close approaches. The idea of using a Hamiltonian splitting into Kepler problems plus perturbations was used, for example, in Wisdom & Holman (1991), for *smooth* planetary dynamics not involving close approaches of bodies.

Consider the case of a perturbed two-body problem with Hamiltonian

$$H = \tfrac{1}{2}|p|^2 - (1/|q|) + \hat{H}(p, q). \tag{5.1}$$

Here we assume that $\hat{H}$ is a small perturbation.

One approach is to split H into the Kepler part and the perturbation, solving first the one with the KS transformation and the other with some symplectic integrator. That is, we set $\bar{H} = \frac{1}{2}|p|^2 - (1/|q|)$, and use the symmetric splitting

$$\exp \Delta t H = \exp \tfrac{1}{2}\Delta t \bar{H} \circ \exp \Delta t \hat{H} \circ \exp \tfrac{1}{2}\Delta t \bar{H} + O(\Delta t^3),$$

where $\exp tH$ is simply notation for the time t flow map of the Hamiltonian H. We then solve $\bar{H}$ by introducing new variables Q, P and integrating the reparametrized system

$$\tilde{H} = |Q|^2(\bar{H} - \bar{H}_0). \tag{5.2}$$

In standard practice (Aarseth 1985), non-symplectic non-reversible methods would be used to integrate (5.1). In general it is found necessary to employ some sort of variable step-size procedure in addition to the use of regularization.

We also found it necessary to incorporate a variable step size, but we do so in a time-reversible way, using an outer Sundman transformation together with the adaptive Verlet method to perform our integration. For reasons discussed in the next section, we use a Sundman transformation of the form

$$g = \frac{1}{1 + |q|^{-1.5}}.$$

We will refer to this general approach as the reversible adaptive regularization or RAR method.

As a first experiment, we solved the perturbed Kepler problem with Hamiltonian

$$H = \tfrac{1}{2}|p|^2 - \frac{1}{|q|} - \frac{1}{|q - q_1|},$$

viewed as describing a moving body around a fixed body located at the origin, in the presence of another fixed distant body (at q_1).

Placing the disturbing body at $q_1 = (0, 0, 5)$, we integrated what would be a moderately high eccentricity orbit for the unperturbed system using initial conditions $q(0) = (1.0, 0.0001, 0.0)$, $p(0) = (-1.0, 0.0, 0.0)$.

Graphs of the xy- and xz-projections of the trajectory are shown in figure 5 for an integration on $[0, 1000]$. The full orbit appears to be quasi-periodic and is built up as follows in the xz-projection: first a sequence of Kepler orbits is constructed

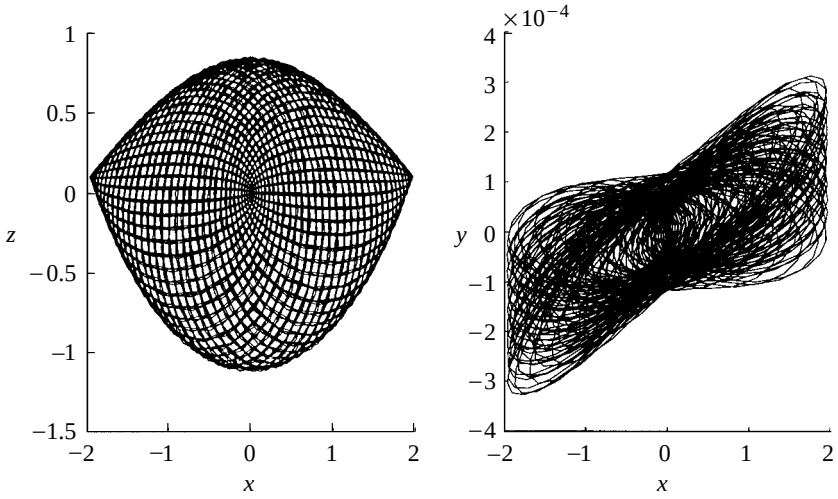

Figure 5. Views of the orbit: the disturbed Kepler problem.

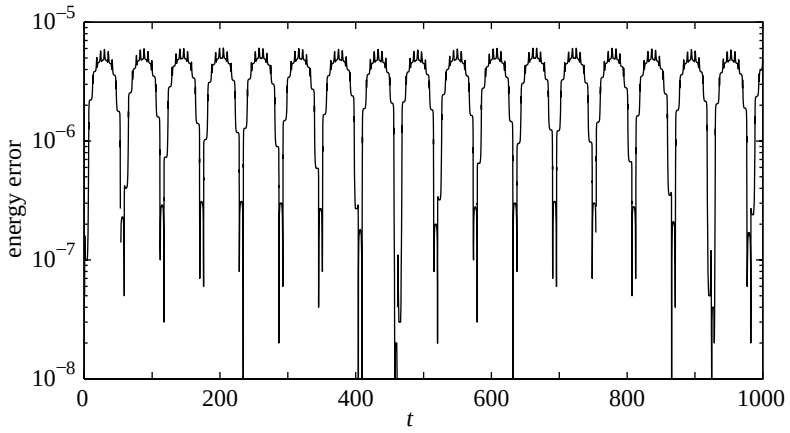

Figure 6. Energy errors for $\Delta\tau = 0.01$.

on the right half of the nucleus, then the process is repeated on the left half. In each such basic cycle, the successive orbits vary from moderately eccentric to nearly circular (which marks the transition to the other side of the diagram). There is also a small oscillating precession visible in the xy-plane projection. A graph of the energy error versus time is shown in figure 6. Note that the energy is highly stable and that there are no large spikes, despite rather close approaches to the origin (within about 0.001). The quasi-periodic character of the motion is well resolved and there is no apparent systematic drift of energy.

The solution of the Kepler problems in the RAR scheme requires the accurate recovery of the time variable (via a quadrature) and inversion of the time transformation at each step if the step is to remain symplectic and the overall method reversible. In an effort to avoid this cost, we tried methods that reverse the order of time and coordinate transformations, i.e. first perform a Poincaré transformation

$$\tilde{H} = |q|(\bar{H} + \hat{H} - H_0). \tag{5.3}$$

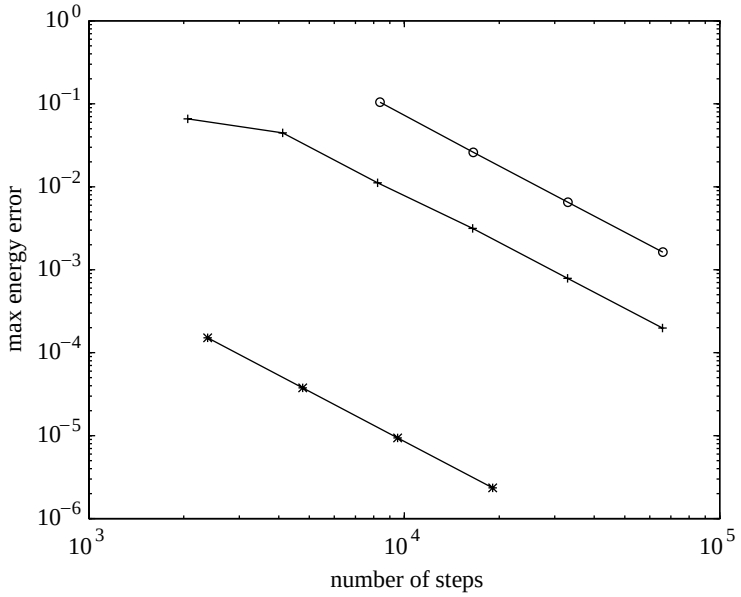

Figure 7. Comparison of work with energy for three methods: (1) (–○–), adaptive Verlet (no regularization); (2) (–+–), time transformation followed by splitting; (3) (–∗–), the RAR method.

We can then split the Hamiltonian into a Kepler part and a perturbation:

$$\tilde{H} = \tilde{H}^{(1)} + \tilde{H}^{(2)}, \qquad \tilde{H}^{(1)} = |q|(\bar{H} - H_0), \qquad \tilde{H}^{(2)} = |q|\hat{H}. \tag{5.4}$$

The individual terms are then integrable successively: $H^{(1)}$ by introducing the KS coordinate transformation and $H^{(2)}$ either by exact integration or by an appropriate numerical scheme. The key point is that both parts of the Hamiltonian are integrated in the same fictive time variable, so they are automatically synchronized and there is no need to invert the time transformation; the computation is thus completely explicit.

However, this method did not compare favourably with the RAR method. When we integrated the disturbed Kepler problem, we still observed the noticeable spikes in energy present in fixed step-size and unregularized variable step-size simulations, although these were somewhat milder than before. The additional use of a Sundman transformation had little effect. The problem appears to be due to the fact that the value H_0 is the total energy of the system, not the energy of just the Kepler part in the vicinity of the close approach. During the close approach, this perturbation is significant and results in qualitatively incorrect dynamics.

Given that the RAR method can essentially stabilize the energy with respect to collisions, we see little advantage in using the alternative scheme.

We place the different schemes mentioned so far into perspective by constructing a work–energy diagram (figure 7), which compares the efficiencies of (1) the adaptive Verlet (unregularized) method with $g = (1+|q|^{-2})^{-1}$; (2) the modified scheme based on time transformation followed by splitting (5.4); and (3) the RAR method with $g = (1+|q|^{-1.5})^{-1}$. Each point in the diagram represents one complete approximate trajectory on $[0, 100]$, requiring the indicated number of time-steps and producing the indicated maximum energy error. While the cost of a time-step is not the same

for each of the methods, the additional work to perform coordinate transformations and to solve the scalar quartic polynomials required by the fast Kepler solver is easily justified by the huge reduction in numbers of time-steps needed for given accuracy.

The remarkable performance improvement obtainable with the use of the regularizing transformation makes the procedure indispensable for perturbed Kepler motion. The combination of this procedure with reversible adaptive methods enables the efficient simulation of long-time-scale phenomena with little degradation of quasi-periodic structure, as we will see in the next sections.

6. Atomic dynamics

Atomic dynamics can be handled using a generalization of the RAR method. This is possible because each electron generally participates in only two types of encounters: (1) collisions with the nucleus; and (2) interactions with the other electrons (or other perturbative forces). In this section, we outline an RAR-based algorithm for treating arbitrary atoms. Details of the algorithm and an extension to treat applied electromagnetic fields may be found in Leimkuhler (1998).

The Hamiltonian for the atomic problem is, in standard atomic units and in the absence of fields,

$$H = \sum_{i=1}^{N} \tfrac{1}{2}|p_i|^2 - \sum_{i=1}^{N} \frac{k}{|q_i|} + \sum_{i=1}^{N-1} \sum_{j=i+1}^{N} \frac{1}{|q_i - q_j|},$$

where k is the charge on the nucleus. This Hamiltonian splits into $N+1$ parts:

$$H^{(i)} = \tfrac{1}{2}|p_i|^2 - \frac{k}{|q_i|}, \quad i = 1, \ldots, N,$$

$$V_{\mathrm{e-e}} = \sum_{i=1}^{N-1} \sum_{j=i+1}^{N} \frac{1}{|q_i - q_j|}.$$

Each of the Kepler Hamiltonians can be integrated using the fast Kepler solver of § 4, while the electron interaction term $V_{\mathrm{e-e}}$ is exactly integrable since it depends only on q.

The last component is the incorporation of a reversible step-size variation procedure. The actual time-step needs to be decreased according to the difficulty of the Kepler problems (i.e. when $|q_i|$ becomes small), since these become more sensitive to the perturbing forces during close approach. A second problem has to do with electron–electron interactions, which can occasionally lead to very strong forces, especially if one electron has recently undergone a strong acceleration via the Coulombic potential. Both of these difficulties are remedied by the use of an outer time transformation of the Sundman type.

(a) *A Sundman transformation for atomic systems*

The design of this time transformation is somewhat tricky. We considered various controls based on the two position-dependent indicators (1) $r_{\mathrm{en}} = \min_i |q_i|$, and (2) $r_{\mathrm{ee}} = \min_{i \neq j} |q_i - q_j|$, of the form

$$g(q) = \frac{1}{r_{\mathrm{en}}^{-a} + r_{\mathrm{ee}}^{-b} + 1}. \tag{6.1}$$

Actually, a variety of different control strategies were explored, but others generally were less reliable; the suggested control proved to be remarkably robust when applied to a wide range of problems. There are good reasons for the choice of each term in (6.1), and the optimal powers a and b can be justified on the grounds of model problems and numerical experiments.

(i) *Electron–electron interactions*

The electron–electron interactions are not treated with any regularization other than the time transformation itself. We can gain insight into this term by considering the purely repulsive one-degree-of-freedom problem with the Hamiltonian

$$H = \tfrac{1}{2}p^2 + (1/q), \quad q > 0. \tag{6.2}$$

We follow the approach given in Bond & Leimkuhler (1998) to obtain an appropriate time transformation for solving this model problem.

After a time-rescaling $g = q^\beta$, the equations of motion for (6.2) are

$$\dot{q} = q^\beta p,$$
$$\dot{p} = q^{\beta-2}.$$

Along an orbit, the material point starts from a distant point (momentum $p_{-\infty}$) and approaches the point of collision $q = \bar{q}$. During a short time-interval, the momentum changes sign and the particle position tends to infinity with asymptotic velocity $p_{+\infty} = -p_{-\infty}$. We next calculate the approximate duration of the collision.

First observe that, far from the wall, the energy is all in the kinetic part, so we have

$$|p_{\pm\infty}| = \sqrt{2E},$$

where E is the constant total energy. At the point of collision, on the other hand, $p = 0$ and $q = \bar{q}$, implying that

$$1/\bar{q} = E.$$

This allows us to solve for $p_{\pm\infty}$ in terms of $\bar{q}$:

$$|p_{\pm\infty}| = \sqrt{2}E^{1/2} = \sqrt{2}\bar{q}^{-1/2}. \tag{6.3}$$

Near the point of close approach, the positional motion slows, almost to a stop, while the velocity changes sign very suddenly according to the equation

$$\dot{p} \approx \alpha\bar{q}^{\beta-2};$$

thus, with τ the total time for this collision,

$$p_{+\infty} - p_{-\infty} \approx \bar{q}^{\beta-2}\tau.$$

But since $p_{-\infty} = -p_{+\infty}$ and using (6.3), we have

$$2\sqrt{2}\bar{q}^{-1/2} \approx \bar{q}^{\beta-2}\tau,$$

or

$$\tau \approx 2\sqrt{2}\bar{q}^{-\beta+3/2} = 2\sqrt{2}E^{\beta-3/2}.$$

We would like to use a value of β for which the *collision time is independent of the strength of the collision*. This evidently occurs for $\beta = \frac{3}{2}$. With this choice, the

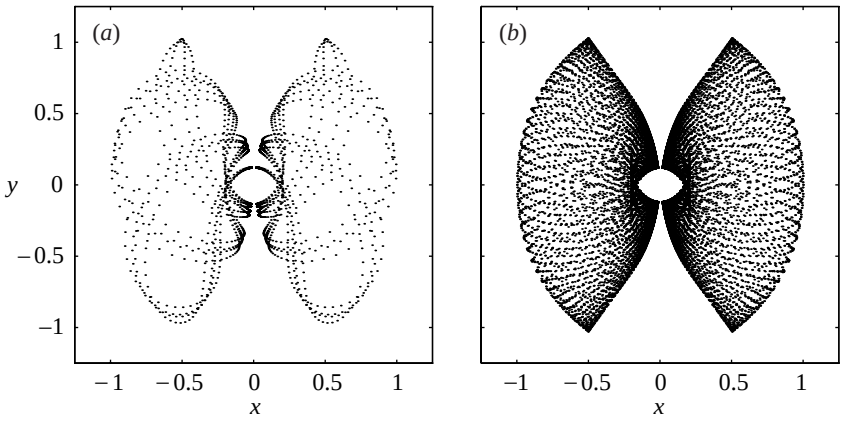

Figure 8. The first test orbit for helium, near a Langmuir orbit, for which the time-step selection is dominated by electron–electron interactions: (a) to $T = 30$; (b) to $T = 300$.

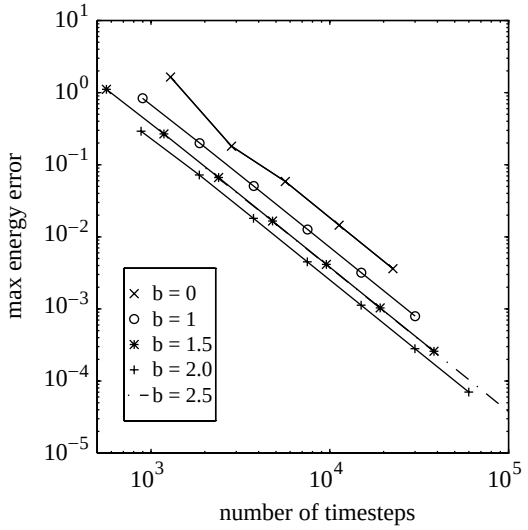

Figure 9. Work–energy diagrams comparing different values of b.

stronger collisions are 'slowed down' in the rescaled time so that they evolve on the same fictive time-scale as weak collisions.

To test the design of the term based on the electron–electron potential, we used the orbit beginning from the initial conditions $q_1 = (1, 0, 0)$, $q_2 = (-1, 0, 0)$, and $p_1 = p_2 = (0, 1, 0)$. The two electrons follow symmetric orbits in the left and right half-planes consisting of long smooth motions punctuated by varying strength e–e-type collisions near the y-axis (the motion is shown in figure 8). This orbit is related to the Langmuir periodic orbit (Steckel & Jaffe 1998).

Fixing $a = 1.5$, we computed several trajectories on $[0, 30]$ for different values of b ($b = 0.0, 1.0, 1.5, 2.0, 2.5$) and of the step size; the resulting work–energy diagrams for each value of b are shown in figure 9. Clearly, there is a substantial gain in efficiency from involving r_{ee} in the control. Although the optimal value in this experiment

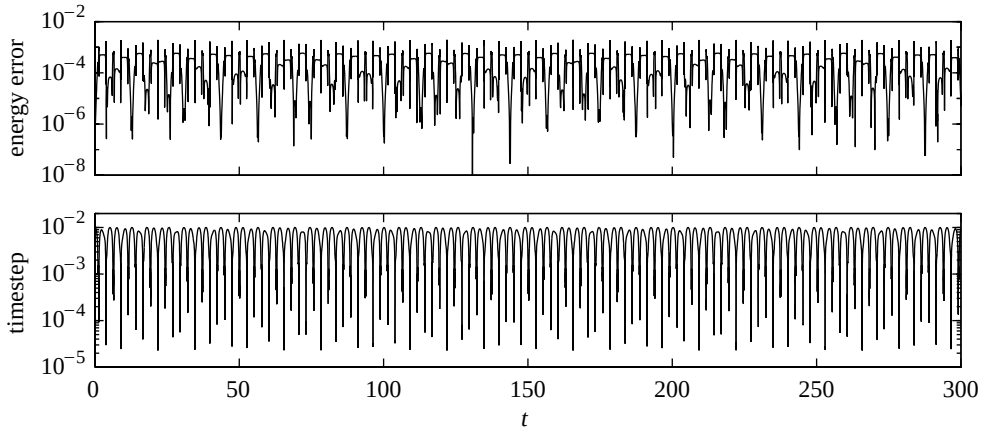

Figure 10. The energy errors and time-step variation observed for $b = 2$, $\Delta t_0 = 0.01$.

occurs at around $b = 2$—a discrepancy with our theoretical discussion—the results for $b = 1.5$ are similar. The resulting energy error and step-size graphs are shown in figure 10. Additional discussion and examples may be found in Bond & Leimkuhler (1998).

(ii) *Electron–nucleus interaction*

For the attractive electron–nucleus interaction, we take another point of view, considering the stability of the Kepler problem with respect to perturbations. The equations of planar Kepler motion are

$$\dot{q} = p,$$
$$\dot{p} = -q/|q|^3.$$

The variational equations describe the change over time in a perturbation evolved along a given trajectory by

$$\frac{\mathrm{d}}{\mathrm{d}t}\begin{bmatrix}\delta q\\ \delta p\end{bmatrix} = \begin{bmatrix}0 & 1\\ -\dfrac{1}{|q|^3}I + 3\dfrac{qq^{\mathrm{T}}}{|q|^5} & 0\end{bmatrix}\begin{bmatrix}\delta q\\ \delta p\end{bmatrix} =: A(q)\begin{bmatrix}\delta q\\ \delta p\end{bmatrix}.$$

We consider the behaviour in the vicinity of $\bar{q}$, the point of close approach along the orbit. At this point, the linearization approximately describes the motion, since the rapidly changing momentum does not appear in $A(\bar{q})$.

The eigenvectors and eigenvalues of $A = A(\bar{q})$ are

$$\xi_{1,2} = \begin{bmatrix}\bar{q}^{\perp}\\ \lambda_{1,2}\bar{q}^{\perp}\end{bmatrix}, \qquad \lambda_{1,2} = \pm \mathrm{i}|\bar{q}|^{-3/2},$$
$$\xi_{3,4} = \begin{bmatrix}\bar{q}\\ \lambda_{3,4}\bar{q}\end{bmatrix}, \qquad \lambda_{3,4} = \pm\sqrt{2}|\bar{q}|^{-3/2},$$

where $q^{\perp}$ is the orthogonal complement to q.

Due to the extreme close approach in the attractive coulombic potential, the positive eigenvalue acting in the transverse direction to the orbit is potentially excessively

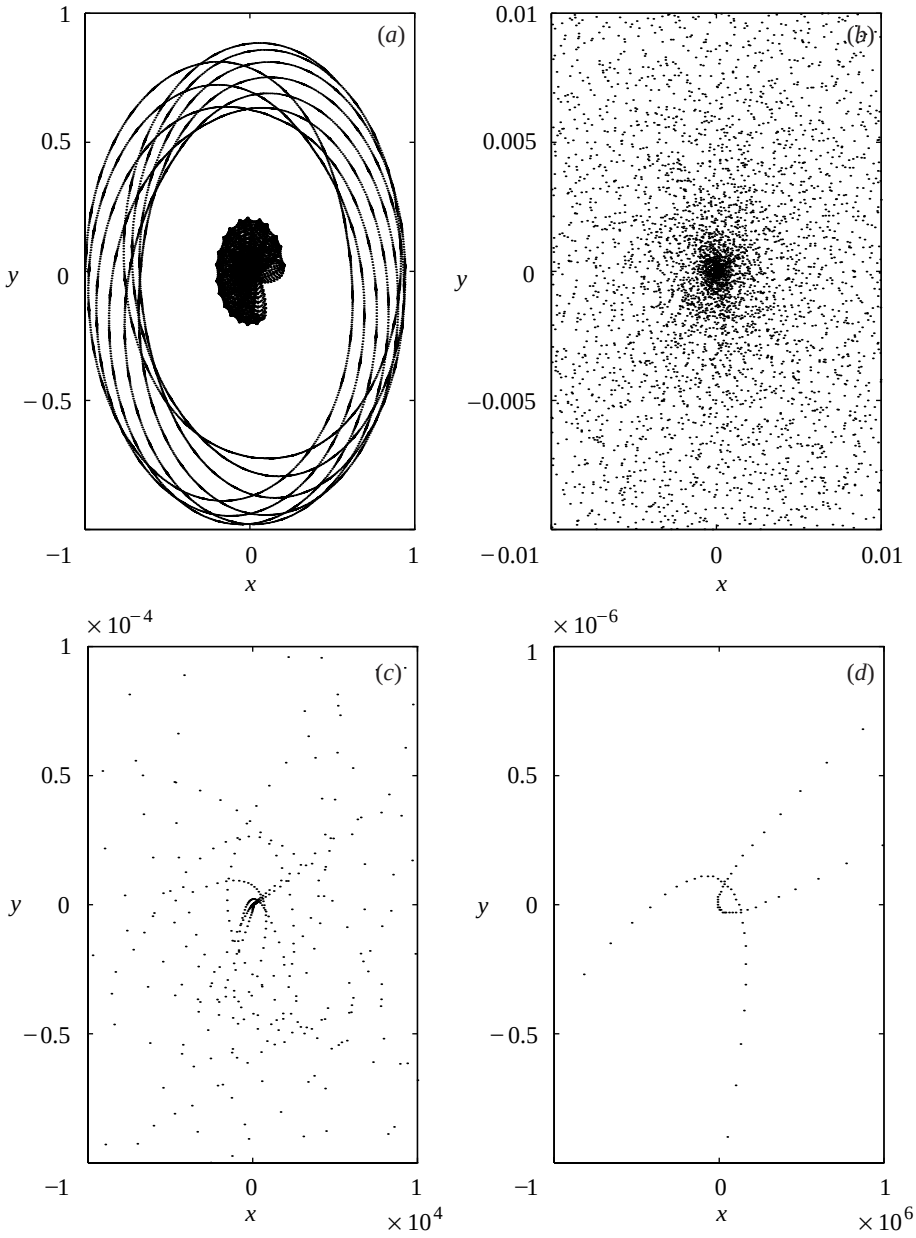

Figure 11. The second test orbit for helium. Here the time-step is dominated by close approaches to the nucleus by the inner electron.

large. It can introduce an instability if excited by the numerical process. Let $\hat{\Phi}$ represent the propagator in one step. We have

$$\hat{\Phi} \approx \exp A(\bar{q})\Delta t,$$

with a principal unstable eigenvalue of

$$\gamma := \exp \sqrt{2}|\bar{q}|^{-3/2}\Delta t.$$

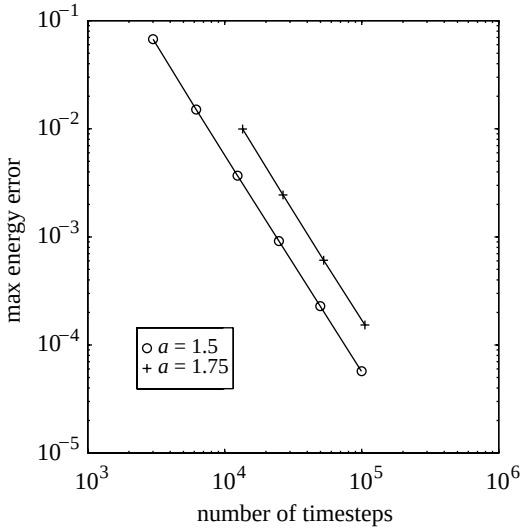

Figure 12. Work–energy diagrams comparing two different values of a; the computation was impossible to carry out for smaller values of a due to instability.

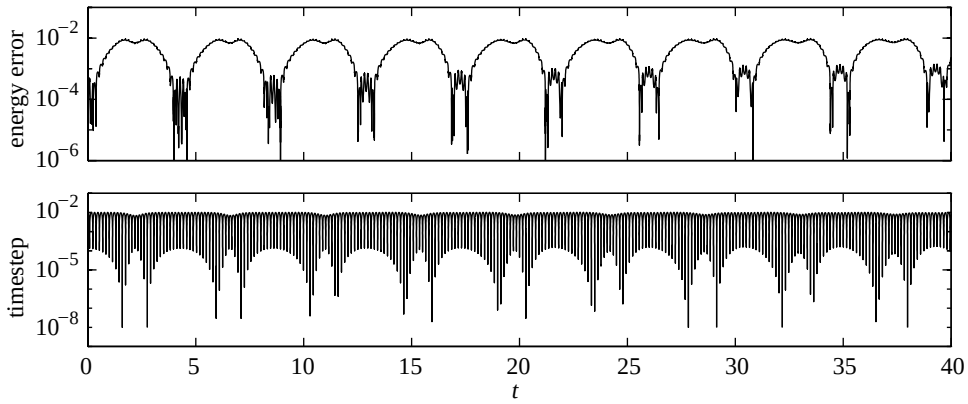

Figure 13. The energy errors and time-step variation observed for $a = 1.5$, $\Delta t_0 = 0.01$.

To control the potential for instability, it is thus necessary to limit the step size with

$$\Delta t \sim |\bar{q}|^{3/2} \Delta\tau$$

during the close approaches. In this way, the growth factor γ is independent of q and limited to

$$\gamma \sim 1 + O(\Delta\tau).$$

To test the design of the term based on the electron–nucleus potential, we used the orbit shown in figure 11. Here the first electron is started in an inner orbit, with $q_1 = (0.2, 0, 0)$, $p_1 = (0, 1, 0)$, while the second electron begins with $q_1 = (1, 0, 0)$, $q_2 = (0, 1, 0)$. The motion of the inner electron is strongly perturbed by the outer body, and the result is an essentially ergodic motion within a bounded region. The electron makes many very close approaches to the nucleus which would, if not resolved using

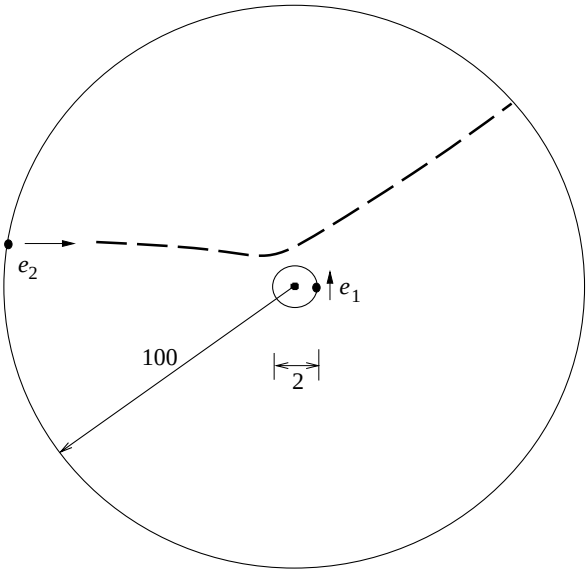

Figure 14. Scattering of He^+.

the regularizing transformation, be essentially impossible to integrate numerically. Note in particular the appearance of Keplerian orbits during very close approach.

We conducted a sequence of experiments, fixing $b = 2.0$ and varying a. In this case, it proved impossible to integrate with values of $a < 1.5$ (the step scaling factor ρ tended to infinity, indicating instability of the integration process); this agrees with the observations made for the Kepler problem. For $a = 1.5$, on the other hand, the integration was very robust, and integration could also be carried out for larger values of a. We compare $a = 1.5$ and $a = 1.75$ in figure 12, showing the superiority of the lower value of a. For higher values of a, the results were substantially worse. With $a = 1.5$, the variations in time-step and the corresponding well-behaved energy error are shown in figure 13.

The energy variation is relatively moderate in this example, with the 'peaks removed' from the corresponding fixed step-size energy behaviour.

7. Application: He^+ scattering

Gu & Yuan (1993) investigated the classical planar scattering of an electron from He^+. Using symbolic dynamics to organize the trajectories, they investigated escape rates and chaotic intermixing. Instead of using the KS transformation, as here, the authors describe an ad hoc integration method which (1) does not integrate the close approach (trajectories are tracked only to within about 10^{-5} of the nucleus); and (2) uses a standard variable-step Runge–Kutta method.

Our experiments are not precisely identical to those of Gu & Yuan (1993) but are essentially equivalent. We used the same energies for each particle, and similar initial orbits. The only difference was in the exact configuration of the distant electron at time $t = 0$. In our experiment, the far electron is fired from a point on the circle of radius $R = 100$: $q_2(0) = (-\sqrt{R^2 - \beta^2}, \beta)$ with $p_2 = (0.65, 0)$, with the inner electron started from initial data $q_1(0) = (0.833, 0)$, $p_1(0) = (0, 1.55)$. The situation is shown

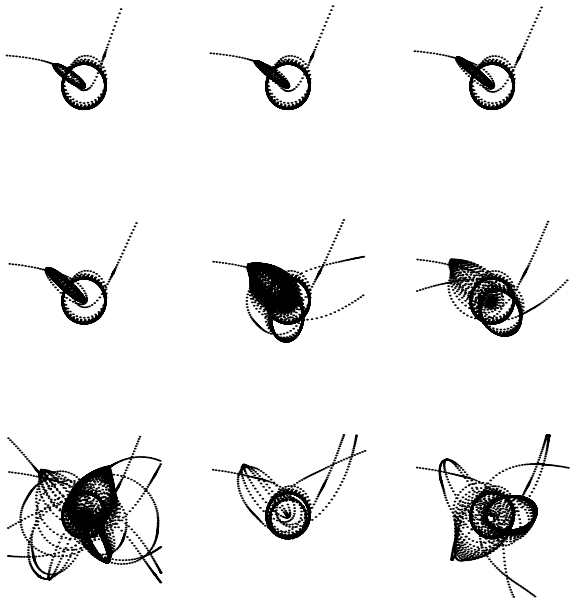

Figure 15. Scattering diagrams for the collisional region $(x, y) \in [-3, 3] \times [-3, 3]$.

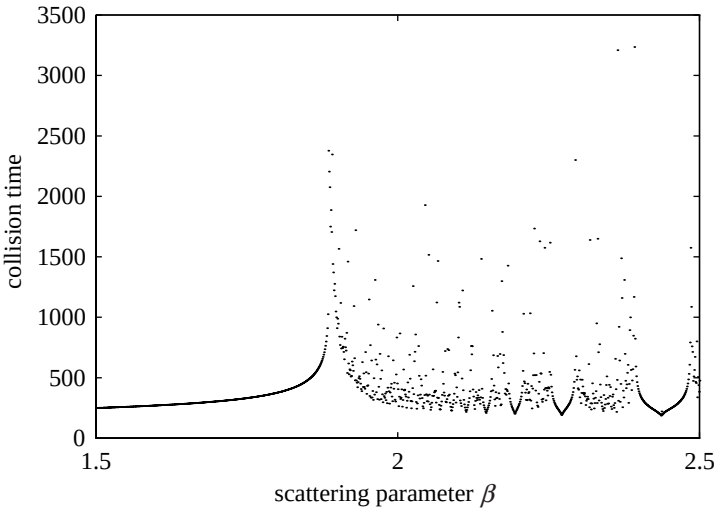

Figure 16. Collision times for $\beta \in [1.5, 2.5]$, $\Delta\tau = 0.01$.

diagrammatically in figure 14. In Gu & Yuan (1993), the parameter β is obtained by simulating the motion of an electron in unit-charge coulombic field up to the circle of radius R from an unspecified distant point; this also results in a very slight change in p_2; the difference in initial data is qualitatively inconsequential, effectively summarized by a slight shift in β. The computation is stopped following collision after one of the electrons reaches the circle of radius R, at which point the total collision time T_c is recorded.

We first performed a series of 1000 computations with $\Delta\tau = 0.01$, graphing T_c as a

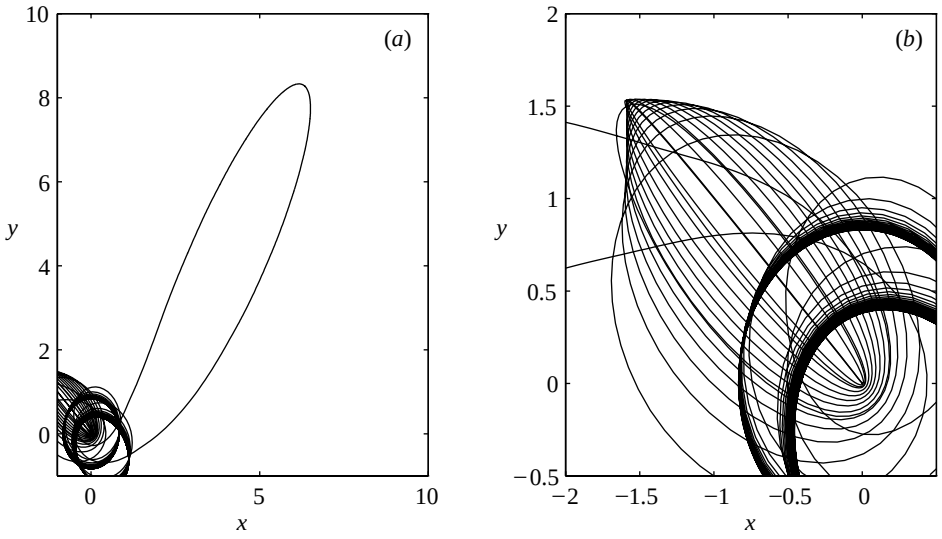

Figure 17. Close-ups of orbit for $\beta = 2.1$ for (a) a long bounded excursion and (b) corresponding precessing elliptical orbits of the inner electron.

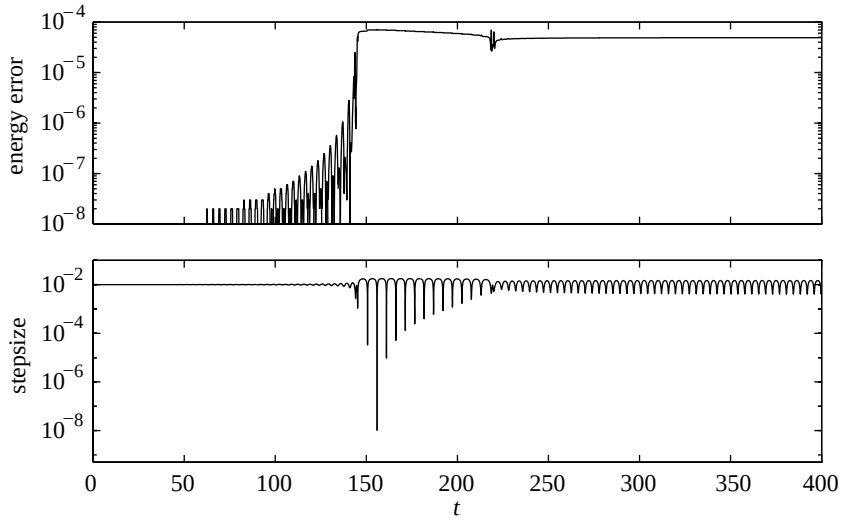

Figure 18. Energy error (upper graph) and step-size variation (lower) for $\beta = 2.1$, $\Delta\tau = 0.01$.

function of the scattering parameter $\beta \in [1.5, 2.5]$. Scattering diagrams for $\beta = 1.5$–2.3 in increments of 0.1 are shown in figure 15. Intervals in β of smoothly varying T_c are intermixed with chaotic regimes (figure 16). Large collision times are associated to long bounded excursions by one or the other electron (figure 17a). During such an excursion, the inner electron path is a series of short-period precessing elliptical orbits (slowly perturbed Kepler motion), often highly eccentric (figure 17b). The energy error increases markedly at the instant when the scattering electron arrives near the unit circle. This rise in energy is not unexpected since the trajectory becomes

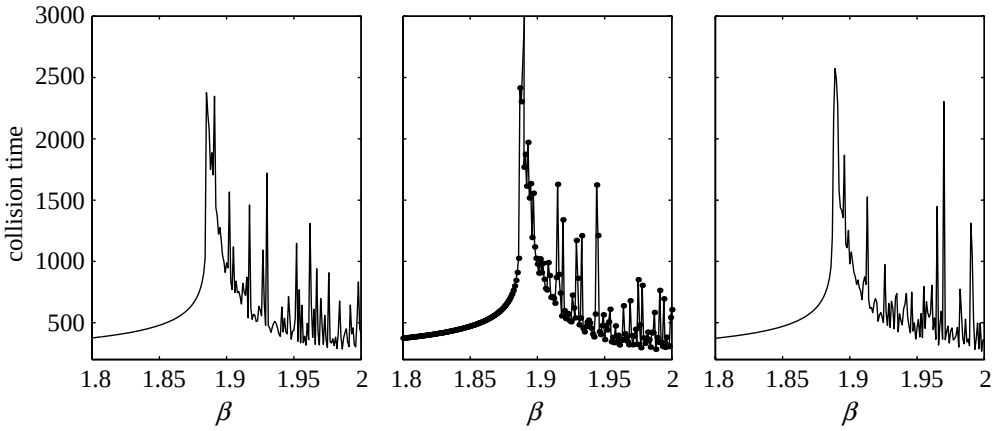

Figure 19. Collisions times converge only in the smooth regime: (*a*) $\Delta\tau = 0.01$; (*b*) $\Delta\tau = 0.005$; (*c*) $\Delta\tau = 0.0025$.

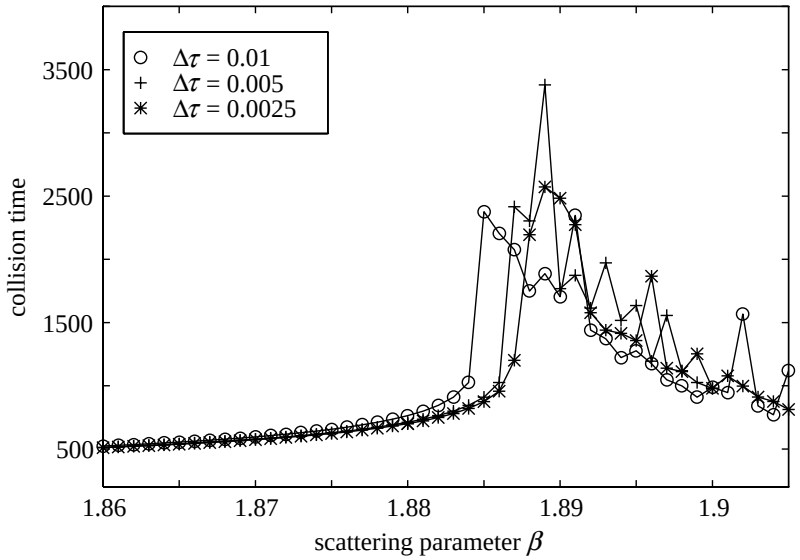

Figure 20. Superposition of graphs in figure 19.

markedly more difficult to integrate at this instant. Figure 18 shows the energy error and step size for the trajectory with $\beta = 2.1$. A reduced fictive time-step $\Delta\tau$ in the smooth regime correctly reduces the error by the square of the reduction factor (second-order integration); however, this does not automatically hold in the chaotic regime, since a small change in the time-step may lead to a drastic change in the solution behaviour (and potentially worse energy error).

Gu & Yuan (1993) relied on the topological features of orbits computed in the chaotic regimes to calculate 'escape rates from the chaotic repellers'. The numerical problem becomes more difficult in the chaotic regime, where many close approaches increase the sensitivity of the solution to small perturbations; nonetheless, the reversible adaptive regularization is generally able to produce reasonable trajectories,

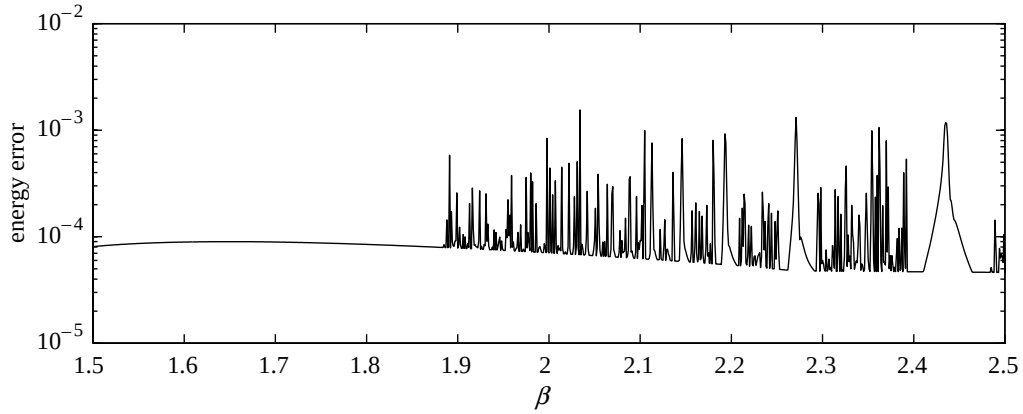

Figure 21. Energy errors as a function of the scattering parameter β for $\Delta\tau = 0.01$.

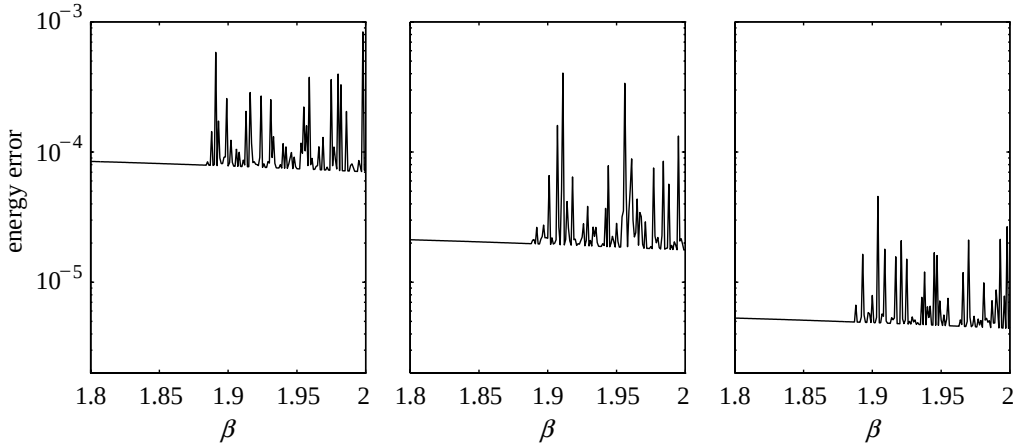

Figure 22. Energy errors by step size: (*a*) $\Delta\tau = 0.01$; (*b*) $\Delta\tau = 0.005$; (*c*) $\Delta\tau = 0.0025$.

with maximum energy error reasonably controlled for most trajectories in both the smooth or chaotic intervals (figure 21). Focusing on the subinterval $[1.8, 2.0]$, we observed that reduction of the step size did lead to apparent convergence of T_c in the smooth subintervals (figure 20), but not in the chaotic regime where the extreme sensitivity of the calculation renders the individual orbits essentially uncomputable in the deterministic sense (figure 19), despite the fact that the trajectory energy errors are converging to zero (figure 22).

This example illustrates one of the most important reasons for using structure-preserving integrators. In the smooth regime, almost any integrator can achieve reasonable results on a fixed time-interval with a sufficiently small time-step. This can be viewed as a direct consequence of the convergence of the method. On the other hand, *in the chaotic regime, nothing can be said regarding the global error of a trajectory*, and we are forced to rely on other properties of the integrator in question (such as preservation of physical properties of the dynamical system) to argue for the validity of our computation.

8. Conclusion

A reversible adaptive regularizing scheme for perturbed Kepler problems and certain types of classical N-body problems has been presented. This method uses a special Sundman transformation, the adaptive Verlet method, KS regularization, and a fast Kepler solver. The resulting algorithm performs well in the examples looked at. What has not been shown is how to use these methods in problems with three-body close approaches; this remains an open challenge.

For useful suggestions and discussions regarding regularization, the author thanks Sverre Aarseth (Cambridge Institute of Astronomy). For helpful discussions on nonlinear dynamics, the author thanks Robert MacKay (DAMTP/Nonlinear Centre). For suggestions and discussions regarding the applications, the author thanks Gregor Tanner (Hewlett-Packard BRIMS) and Colm Whelan and Jens Rasch (DAMTP/Atomic Theory Group). The author also warmly acknowledges the considerable moral support provided by Arieh Iserles (DAMTP) and the successful efforts of Mike Powell and David Crighton (DAMTP) to arrange financial support at unreasonably short notice. This research was supported by NSF grants DMS-9303223 and DMS-9627330 and the DAMTP.

References

Aarseth, S. J. 1985 Direct methods for N-body simulation. In *Multiple time scales* (ed. J. U. Brackbill & B. I. Cohen). New York: Academic.

Barth, E., Leimkuhler, B. & Reich, S. 1999 A semi-explicit, variable stepsize, time-reversible integrator for constrained dynamics. *SIAM J. Sci. Comput.* (In the press.)

Benettin, G. & Giorgilli, A. 1994 On the Hamiltonian interpolation of near-to-the-identity symplectic mappings with application to symplectic integration algorithms. *J. Statist. Phys.* **74**, 1117.

Benvenuto, F., Casati, G. & Shepelyansky, D. 1997 Dynamical localization: hydrogen atoms in magnetic and electrical fields. *Phys. Rev.* A **55**, 1732.

Bond, S. & Leimkuhler, B. 1998 Time transformations for reversible variable stepsize integration. *Numer. Algorithms* **19**, 55–71.

Bulirsch, R. & Stoer, J. 1980 *Introduction to numerical analysis*. New York: Springer.

Calvo, M. P. & Hairer, E. 1995 Acurate long-term integration of dynamical systems. *Appl. Numer. Math.* **18**, 95.

Calvo, M. P. & Sanz-Serna, J. M. 1993 The development of variable stepsize symplectic integrators with application to the two-body problem. *SIAM J. Sci. Comput.* **14**, 936.

Cirilli, S., Hairer, E. & Leimkuhler, B. 1999 Asymptotic error analysis of the Adaptive Verlet method. *BIT* **39**, 25–33.

Ezra, G., Richter, K., Tanner, G. & Wintgen, D. 1991 *J. Phys.* B **24**, L413.

Frank, J., Huang, W. & Leimkuhler, B. 1997 Geometric integrators for classical spin systems. *J. Comput. Phys.* **133**, 160.

Funato, Y., Hut, P., McMillan, S. & Makino, J. 1996 Time-symmetrization of Kustaanheimo–Stiefel regularization. *Astrophys. J.* **112**, 1697.

Ge, Z. & Marsden, J. 1988 Lie–Poisson Hamilton–Jacobi theory and Lie–Poisson integrators. *Phys. Lett.* A **133**, 134.

Gonzales, O. & Stuart, A. M. 1996 Remarks on the qualitative properties of the modified equations. Preprint, SCCM program, Stanford University.

Gu, Y & Yuan, J.-M. 1993 Chaotic scattering of electrons with He^+. *Phys. Rev.* A **47**, R2442.

Gutzwiller, M. 1990 *Chaos in classical and quantum mechanics*. New York: Springer.

Hairer, E. 1994 Backward analysis of numerical integrators and symplectic methods. *Annals Numer. Math.* **1**, 107.

Hairer, E. 1997 Variable timestep integration with symplectic methods. *Appl. Numer. Math.* **25**, 219.

Hairer, E. & Lubich, C. 1999 *Asymptotic expansions and backward analysis for numerical integrators.* IMA Volumes in Mathematics and its Applications. Springer. (In the press.)

Hairer, E. & Stoffer, D. 1997 Reversible long-term integration with variable step sizes. *SIAM J. Sci. Comput.* **18**, 257.

Hairer, E., Nørsett, S. P. & Wanner, G. 1991 *Solving ordinary differential equations*, vol. I. New York: Springer.

Heggie, D. C. 1974 *Cel. Mech.* **10**, 185.

Heggie, D. C. 1988 The N-body problem in stellar dynamics. In *Long-term dynamical behavior of natural and artificial N-body systems* (ed. A. E. Roy). Dordrecht: Kluwer.

Holder, T., Leimkuhler, B. & Reich, S. 1998 Explicit variable stepsize and time-reversible integration. Preprint.

Huang, W. & Leimkuhler, B. 1997 The adaptive Verlet method. *SIAM J. Sci. Comput.* **18**, 239.

Hut, P., Makino, J. & McMillan, S. 1995 Building a better leapfrog. *Astrophys. J.* **443**, L93–L96.

Hut, P., Funato, Y., Kokubo, E., Makino, J. & McMillan, S. 1999 Time symmetrization meta-algorithms. In *Computational astrophysics, Proc. 12th 'Kingston meeting' on Theoretical Astrophysics* (ed. D. A. Clarke & M. J. West). ASP Conference Series. San Francisco, CA: ASP.

Kustaanheimo, P. & Stiefel, E. 1965 Perturbation theory of Kepler motion based on spinor regularization. *J. Reine Angew. Math.* **218**, 204.

Lecar, M. 1968 Comparison of eleven numerical integrations of the same gravitational 25-body problem. *Bull. Astron.* **3**, 91.

Lee, E., Brunello, A. & Farrelly, D. 1997 Coherent states in a Rydberg atom: classical mechanics. *Phys. Rev.* A **55**, 2203.

Leimkuhler, B. 1998 Reversible adaptive regularization methods for atomic N-body problems in applied fields. *Appl. Numer. Math.* **29**.

MacKay, R. S. 1990 Some aspects of the dynamics and numerics of Hamiltonian systems. In *Proc. IMA Conf. on the Dynamics of Numerics and the Numerics of Dynamics* (ed. J. Broomhead & A. Iserles). Cambridge University Press.

McLachlan, R., Quispel, G. R. W. & Turner, G. S. 1998 Numerical integrators that preserve symmetries and reversing symmetries. *SIAM J. Numer. Analysis* **35**, 586–599.

Main, J. & Wunner, G. 1997 Hydrogen atom in a magnetic field: ghost orbits, catastrophes, and uniform semiclassical approximation. *J. Phys.* A **55**, 1743.

Marsden, J. 1992 *Lectures on mechanics.* Cambridge University Press.

Mikkola, S. 1997 Practical symplectic methods with time transformation for the few-body problem. *Celestial Mech. Dynamical Astronomy* **67**, 145.

Noid, D., Gray, S. & Rice, S. 1986 *J. Chem. Phys.* **85**, 2649.

Reich, S. 1999 Backward error analysis for numerical integrators. *SIAM J. Numer. Analysis.* (In the press.)

Richter, K. & Wintgen, W. 1990 *J. Phys.* B **23**, L197.

Richter, K., Tanner, G. & Wintgen, W. 1993 *J. Phys.* A **48**, 4182.

Ruth, R. D. 1983 A canonical integration technique. *IEEE Trans. Nucl. Sci.* **30**, 2669.

Rzazewski, K., Lewenstein, M. & Salieres, P. 1994 Multielectron stabilization of atoms in a laser field: classical perspective. *Phys. Rev.* A **49**, 1196.

Sanz-Serna, J. M. & Calvo, M. P. 1994 *Numerical Hamiltonian problems.* Oxford: Chapman & Hall.

Siegel, C. L. & Moser, J. K. 1971 *Lectures on celestial mechanics.* Berlin: Springer.

Steckel, J. & Jaffe, C. 1998 The bifurcations of the Langmuir orbit in the two-electron atom Hamiltonian systems with three or more degrees of freedom. *NATO ASI series*. Dordrecht: Kluwer.

Stoffer, D. 1995 Variable steps for reversible integration methods. *Computing* **55**, 1.

Warming, R. F. & Hyett, B. J. 1974 The modified equations approach to the stability and accuracy of finite difference methods. *J. Comput. Phys.* **14**, 159.

Wisdom, J. & Holman, M. 1991 Symplectic maps for the N-body problem. *Astron. J.* **102**, 1528.

PHILOSOPHICAL TRANSACTIONS OF THE ROYAL SOCIETY A MATHEMATICAL, PHYSICAL & ENGINEERING SCIENCES

PHILOSOPHICAL TRANSACTIONS OF THE ROYAL SOCIETY A MATHEMATICAL, PHYSICAL & ENGINEERING SCIENCES